Superconducting motors for aircraft propulsion: the Advanced Superconducting Motor Experimental Demonstrator project

Journal of Physics: Conference Series **1590** (2020) 012051 doi:10.1088/1742-6596/1590/1/012051

Superconducting motors for aircraft propulsion: the Advanced Superconducting Motor Experimental Demonstrator project

Francesco Grilli[1], Tara Benkel[1], Jens Hänisch[1], Mayraluna Lao[1]†, Thomas Reis[2], Eva Berberich[2], Simon Wolfstädter[2], Christian Schneider[2], Paul Miller[3], Chloe Palmer[3], Bartek Glowacki[4]‡, Vicente Climente-Alarcon[4], Anis Smara[4], Lukasz Tomkow[4], Johannes Teigelkötter[5], Alexander Stock[5], Johannes Büdel[5], Loïc Jeunesse[6], Martin Staempflin[6], Guillaume Delautre[6], Baptiste Zimmermann[6], Ruud van der Woude[7], Ana Perez[7], Sergey Samoilenkov[8], Alexander Molodyk[8], Enric Pardo[9], Milan Kapolka[9], Shuo Li[9] and Anang Dadhich[9]

[1]Institute for Technical Physics, Karlsruhe Institute of Technology, Karlsruhe, Germany
[2]Oswald Elektromotoren, Miltenberg, Germany
[3]Central Technology Group, Rolls-Royce plc, Derby, United Kingdom
[4]Department of Materials Science and Metallurgy, University of Cambridge, Cambridge CB3 0FS, UK
[5]TH Aschaffenburg University of Applied Sciences, Aschaffenburg, Germany
[6]Air Liquide Advanced Technologies, 2 rue de Clémencière BP 15, 38360 Sassenage, France
[7]Demaco Holland B.V., P.O. Box 4, 1723 ZG Noord-Scharwoude, The Netherlands
[8]SuperOx, Moscow, Russia
[9]Institute of Electrical Engineering, Slovak Academy of Sciences, Bratislava, Slovakia

E-mail: `francesco.grilli@kit.edu`

Abstract. The European Union-funded Advanced Superconducting Motor Experimental Demonstrator (ASuMED) project started in May 2017 with the purpose of demonstrating the benefits of a new, fully superconducting motor for reaching the targets established by the Flightpath 2050 plan. The project aims at a motor power density of 20 kW kg^{-1} using a high-temperature superconducting (HTS) stator. The rotor will use HTS stacks operating like permanent magnets. A highly efficient cryostat for the motor combined with an integrated cryogenic cooling system and associated power converter will be used. This article provides a general overview of the prototype that is currently being assembled and that will be tested soon.

1. Introduction

The unceasing increase of air traffic combined with its fossil fuel consumption and emissions is one of the major environmental issues of our modern world. To remedy this situation, several goals have been set out by the Advisory Council for Aviation Research and Innovation

†M. Lao has recently moved from KIT to another employer.
‡B. Glowacki is also with Institute of Power Engineering, ul. Mory 8, 01-330 Warsaw, Poland.

Figure 1. Mockup of the ASuMED motor presented at the 2019 Hannover Fair.

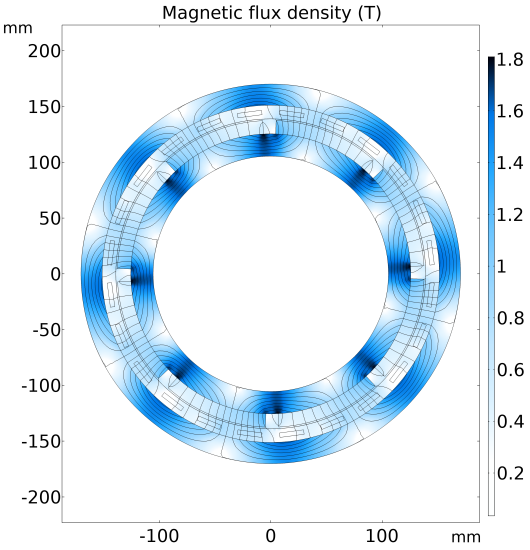

Figure 2. Magnetic field map in the cross section of the ASuMED motor, with permanent magnets in the rotor. In the final design, stacks of HTS tapes will be used.

in Europe (ACARE) in the Flightpath 2050 report [1], in particular reductions in CO_2 by 75 %, NO_x and particulates by 90 %, and noise by 65 % compared to those of year 2000. Focusing on improving already existing aircraft configurations seems to be a difficult path to meet the expected targets. Furthermore, new breakthrough concepts are intensively investigated such as distributed propulsion (DP), which, by opening the aircraft design space, is expected to lead to major reductions in fuel consumption, emissions and noise [2]. Promising great improvements in aircraft efficiency, DP is being studied to meet the Flightpath 2050 targets. However, these goals remain challenging and the DP technology must be lightweight as well as achieve a very high efficiency to reach the expected goals. For large aircraft propulsion, the high-power level requirements make superconducting technology a major enabler for DP. In this context, the ASuMED consortium is building the first fully superconducting motor prototype achieving the power densities and efficiencies needed for hybrid-electric distributed propulsion (HEDP) of future large civil aircraft. This contribution provides an overview of the ASuMED project and a description of the main features of the prototype motor, which is currently being assembled.

2. Motor's requirements and topology

The demonstrator motor requirements are representative of an expected ducted-fan distributed-propulsion aircraft application that operates at a nominal altitude of 40000 ft and cruise speed of 0.8 Mach. A 1 MW rated fan for this application would have a maximum normal rotational speed of approximately 6000 rpm. The assumption is that the motor will be located behind the propulsion fan and drive the fan via an internal shaft. Therefore, the motor diameter could be up to slightly larger than the diameter of the fan hub; 350 mm was chosen as the diameter limit.

With these requirements, the synchronous motor with permanent magnets topology was chosen to obtain the best system performance. The final electro-magnetic layout resulted in a design with 8 poles (corresponding to 400 Hz at 6000 rpm) and a distributed winding system in the stator. Figure 1 shows a mockup of the motor presented at the 2019 Hannover Fair. Figure 2 illustrates the geometry and a magnetic field map in the cross section of the motor.

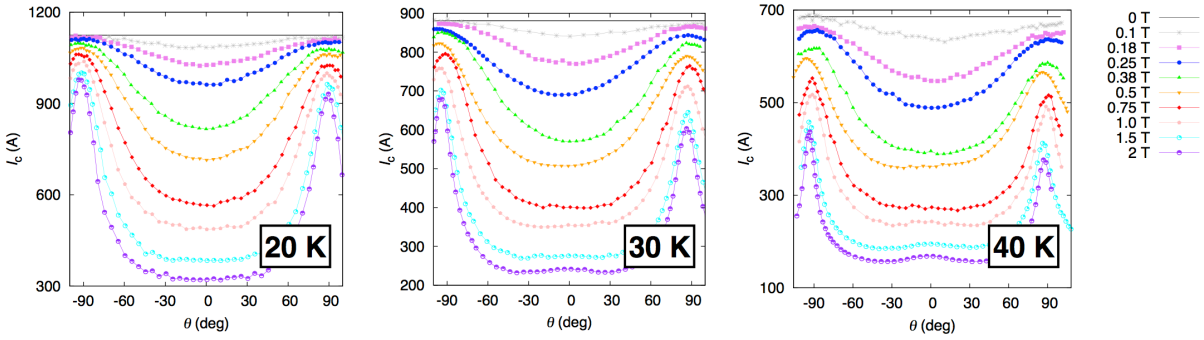

Figure 3. Angle dependence of I_c at 20, 30, 40 K and several magnetic fields of a SuperOx coated conductor sample. 0° refers to the field direction perpendicular to the tape and ±90° corresponds to the direction parallel to the tape surface.

3. Superconducting materials

The coated conductors for the stator coils were developed and supplied by SuperOx [3, 4]. They consist of a 4 mm-wide IBAD-MgO template with several buffer layers, a PLD-grown $GdBa_2Cu_3O_7$ film with additional Cu stabilization of at least 20 µm thickness. The electrical transport properties of the tapes were determined with a 6 T split-coil system for variable temperatures, full sample rotation and currents up to 1.2 kA [5] in the relevant field and temperature range (from 0 to 2 T, from 20 to 40 K). Figure 3 exemplarily shows the angle dependence of I_c of such a coated conductor at three temperatures and several applied fields. During the course of the project, SuperOx improved I_c of their coated conductors by 80 % by introducing $BaSnO_3$ nanoparticles for enhanced flux pinning [6, 7]. These coated conductors were also characterized at certain fields and temperatures (not shown here) and finally used for the motor demonstrator. For the stacks of the rotor, 40 mm mm-wide HTS tapes from Deutsche Nanoschicht were used.

4. AC losses in the stator

In order to estimate the AC losses in the stator's HTS windings, the following approach was taken. The magnetic field and magnetic vector potential maps were calculated by simulating the whole motor with the commercial finite-element program COMSOL Multiphysics (an example is shown in figure 2). For this step, the HTS windings were simulated as blocks of conventional material, the goal being to calculate the temporal evolution of the magnetic flux distribution in the machine (without the details of the current distribution inside the HTS tapes). The field maps – calculated at different time steps of the AC cycle by means of static simulations where time enters as a parameter – were then exported and used as non-uniform applied magnetic field for a separate program based on the minimum electro-magnetic entropy production (MEMEP) method [8], dedicated to the calculation of the AC losses in the HTS windings. More details on this procedure can be found in [9].

The total current flowing in the coils is 7 kA (peak value) at 400 Hz. For a longitudinal length of 18 cm and the angular dependence of I_c shown in figure 3, the average power dissipation in the stator coils is 250, 380, 570 W at 20, 30, 40 K, respectively. These loss values are promising, because they are below 1 % of the motor power. They might also be a bit optimistic, because the model used for the loss calculations assumes a uniform current density along the tape's width. In the analyzed cases, the current flowing in the stator's turns is a small fraction of the tape's critical current and as such it tends to flow near the edge of each tape. In that part of the tape, the local value of J_c could be substantially lower than in the rest of the tape, which would result

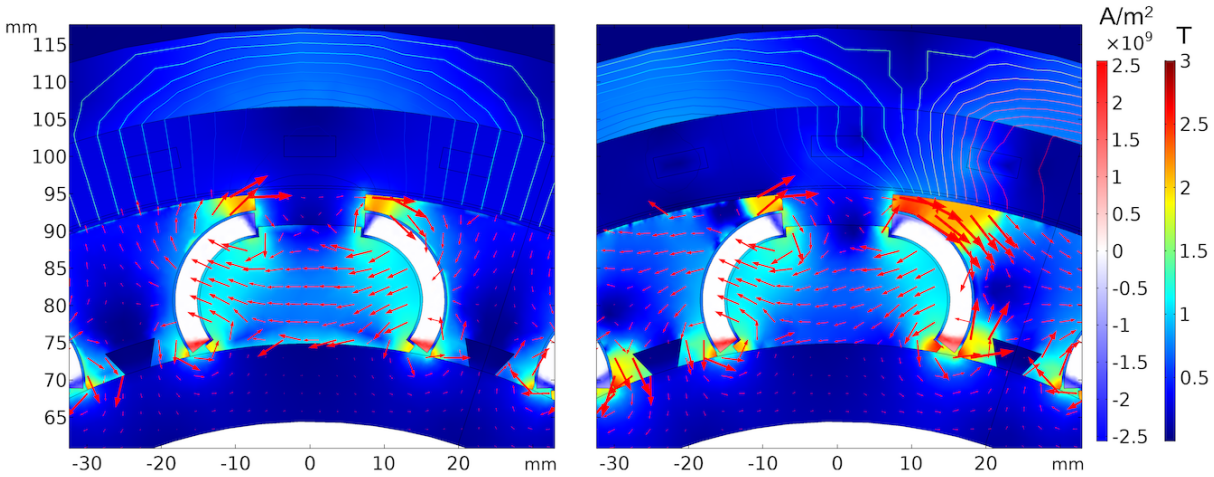

Figure 4. Currents in the stacks and magnetic flux distribution in the ASuMED motor cross section. Left: After magnetization, currents are induced in the stacks, but there are no currents in the stator winding yet. Right: During operation, nominal currents are present in the stator windings, the rotor moves and torque is generated.

in substantially higher losses than in a tape without spatial variation of J_c [10, 11, 12, 13].

5. HTS tape stacks in the rotor

Stacks of wide HTS tape were selected as source of magnetic flux density in the rotor. Once magnetized, these elements would develop the role of permanent magnets. This simplifies the construction of the motor since no current leads are needed in the rotor, an element already quite complex [14]. Among the advantages of using stacks compared to permanent magnets, one can find that the peak magnetic remanent flux can be potentially doubled, and the good mechanical properties provided by the substrate. Compared to bulks of superconducting material, stacks are easier to manufacture, since tapes can be cut, bent and bonded together without impact on their electromagnetic properties. Stacks are not affected by point defects either, as the different layers smooth out their influence, yielding a reproducible magnetic flux density profile. Moreover, unlike bulks, they can be manufactured in more complicated shapes, which allow, for instance, following the curvature of the rotor. Nevertheless, amid the disadvantages of using trapped-flux magnets as a flux source in the rotor of an electrical machine, one must cite the necessity to magnetize them from the stator – if the simplified construction of the rotor is to be maintained – and the perturbations caused by the air gap harmonics in these elements. The latter stem from the fact that since the current loops induced in the stacks are macroscopic, any variations of the magnetic flux density, as the ones caused by the spatial harmonics in a rotating electrical machine, disturb this current flow yielding to demagnetization [15], such as cross-field demagnetization due to ripple fields parallel to the tape. After evaluating several conventional configurations, a novel rotor architecture was developed, in order to favor magnetization from the stator but at the same time protect the stacks from demagnetization. This new layout takes advantage of the mechanical properties of the stacks, enabling a curved C-shape that maximizes their width whilst mechanically joining the different elements of the rotor [16].

Since cross-field demagnetization is a problem of fundamental importance, we studied the cross-field demagnetization process by 3D modeling and measurements in a single flat stack [15]. The modeling used the MEMEP method in 3D, which is able to take the real thickness of the superconducting tape (around 1.5 µm) into account. Modeling results show that it is essential

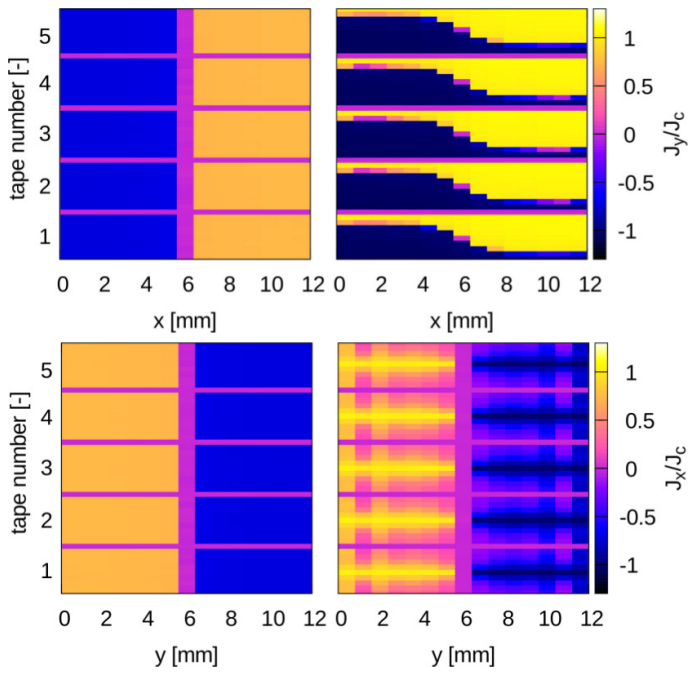

Figure 5. MEMEP 3D modeling of the cross-field demagnetization process of stacks of tapes allows predicting the decay of magnetizing current density in both components of the in-tape current density [15]. Left: configuration after field cooling with applied field in the vertical, z, direction. Right: the same but at the peak of the 10^{th} demagnetizing cycle due to an AC magnetic field in the x direction. Top: in-plane component of **J** perpendicular to the ripple field at the mid-plane of the stack ($y = 6$ mm). Bottom: in-plane component of **J** parallel to the ripple field at the mid-plane of the stack ($x = 6$ mm).

to take the real thickness into account. In addition, 3D modeling is necessary for short stacks, such as experimental samples made of square tapes, in order to take finite length effects into account, as well as the reduction in both in-tape components of the current density (see figure 5). As shown in [15], the simulation results satisfactorily agree with measurements. The remaining discrepancy may be due to force-free effects in the critical current density, which are not included in the model. Further cross-sectional 2D modeling for high number of cycles, up to 2 million (∼1 hour for ripples of 500 Hz), show that for low enough ripple field amplitudes the trapped field does not decay indefinitely, reaching a stable asymptotic value [17]. This is consistent with measurements on a downscaled test motor [18].

6. Cryogenics

The cryogenic topology of the ASuMED motor is based on a dual-cryostat concept, which consists of separate cryostats for the rotor and the stator. A solution in which two cryostats are combined in one motor gives the possibility to use the most suitable technology for both rotor and stator and thus meet the most demanding requirements of the system. Apart from the cryogenic design, an important aspect of the rotor cryostat is the rotating seal between the cooling fluid and the vacuum. Ferrofluidic seals were chosen for this purpose and the first tests show that their performance is acceptable. The stator cryostat is based on a capillary system, which uses liquid hydrogen as the cooling fluid. To achieve the highest cooling capability this contact cooling system is directly integrated into the stator coils.

The rotor cryostat design is to a large extent determined by the cooling concept, which is particularly challenging because of the cryogenic temperatures, the cooling power and the rotating parts. The required 150 W capacity of the rotor cooling system during operation is defined by the heat generation in the superconducting rotor stacks and heat leak into the cryogenic system. The conduction and radiation components of the heat leak were estimated with conventional rule-based methods. In this vacuum insulated system, the convection component can be ignored.

The cooling fluid for the rotor cryostat is helium at 25 K and 2 bar(a) and the rotor HTS stacks

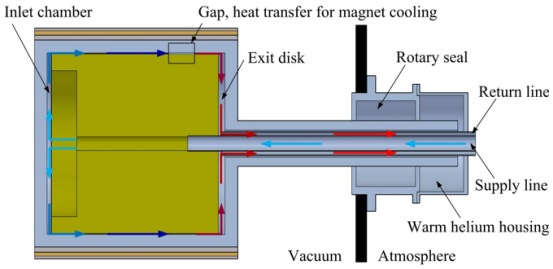

Figure 6. Overview of the externally controlled cooling system for the ASuMED rotor showing the design and main components.

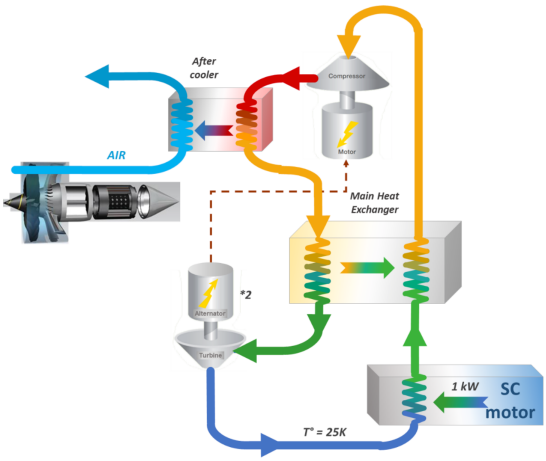

Figure 7. Schematic illustration of the cryocooler cycle for the ASuMED motor.

are designed to work at 30 K. The rotor body is part of the housing for the cryostat, meaning that the cooling circuit is built inside the rotor. A number of alternatives based on different heat transfer mechanisms were considered for the rotor cooling system topology. A conduction based system was the first design concept to be investigated but preliminary analyses showed that the achieved cooling capacity was not sufficient. A forced convection based system was then proposed as a way of improving the heat transfer in the system. A preliminary heat transfer analysis on this configuration showed that this system has the potential to achieve the required cooling power. The forced convection in the system is realized by the forced circulation of the cooling gas through the system. This is the so-called externally controlled cooling system for the ASuMED motor, shown in figure 6, in which gaseous helium is circulated to remove the heat generated in the rotor HTS stacks. This concept is supported by a detailed flow and heat transfer analysis, using the finite element method. Furthermore, experimental validation of the rotor cooling system is expected before the testing of the final demonstrator [14].

During the project, the conceptual study on future integration of cryogenic supply in airborne applications was carried out. In order to cool down the superconducting motor, the cryocooler must produce 1 kW of cold power at 25 K. The biggest challenge was to design a cryocooler (i) light and small enough to be integrated in an aircraft; (ii) with a limited input power to maximize the yield of the whole propulsive chain. The study led to a cryocooler design with a mass of approximately 200 kg (not including the power electronics nor the frame that could be part of the aircraft), mainly using light heat exchangers and an optimized cryocooler cycle. Air is used as hot sink to cool the process fluid and the input power of the cryocooler is smaller than 50 kW (less than 5 % of motor power). A schematic illustration of this cryocooler is given in figure 7. Studies were also performed about the possibility of using liquid methane as hot sink (instead of air as hot sink to cool the process fluid) and liquid hydrogen (used directly to cool the engine, without cryocooler). It was found that the mass of the cooling system can be decreased if liquid methane or hydrogen is also used to produce the electricity that feeds the superconducting motor.

7. Power electronics

For the high requirements for aerospace applications, different inverter topologies were investigated. For the ASuMED project, the dual two-level inverter topology was discovered to be the most promising topology for the application in an aircraft. With its high redundancy,

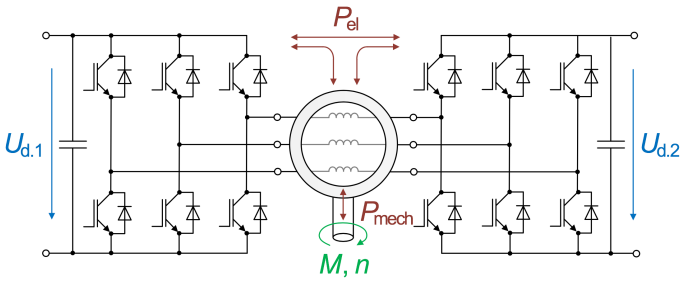

Figure 8. Topology of the three-phase dual two-level inverter.

the inverter is optimally suited for this application. The separated DC-links enable the use of two different energy sources, if desired. In dependency of the DC-link voltage ratio $R_1 = U_{\mathrm{d.1}}/U_{\mathrm{d.2}}$, the dual two-level inverter also has a multilevel behavior. For $r = 1$ a three level, for $r = 2$ a four level, and for $r = 3$ a five level behavior can be achieved [19]. A higher number of voltage levels leads to an increased number of voltage steps for a sinusoidal output voltage. This leads to a better sinusoidal waveform and to a high reduction of harmonics in the output quantities. Consequently, a lower effort for output filters is necessary. The reduced harmonic distortion also leads to lower losses in the motor [20]. Simultaneously, a high number of output voltage steps drastically reduces electro-magnetic interference, so that the inverter decreasingly stresses the aircraft components. This topology also has the advantage of a higher redundancy level compared to a standard three-phase two-level inverter [21]. In case of a failure, it is possible to operate the motor continuously with constant torque but reduced voltage and therefore reduced power. With the separation of the two independent DC power sources, the possibility of choosing different power supplies is given. If one power supply fails, the corresponding inverter has to be shut down, while the other independent inverter remains active. In this case, the motor can operate with the same torque but reduced power resulting in reduced speed. The energy transfer is not limited to flow from the inverters to the motor or vice versa. Energy can also be exchanged between the two inverters throughout the machine windings. This energy flow is controllable and can take place during the normal operation of the motor without affecting its operation. For example, if there is a battery attached to the DC-link of one inverter, this battery can be charged by the second inverter throughout the machine during conventional operation.

The concept of the dual two-level inverter also offers the possibility, if the arrangement of the semiconductor is slightly changed, of operating the superconducting coils optimally with respect to the losses [22]. In combination with a highly dynamic measurement of voltage and current, as it is proposed in [23], this topology can guarantee a safe and reliable operation of the superconductors.

8. Conclusion

This article presented an overview of the ASuMED project, which aims at demonstrating the benefits of a fully superconducting motor for reaching the targets established by the Flightpath 2050 plan. The main characteristics of the motor that is currently being assembled were described, with particular reference to the following aspects: the superconducting materials used in the stator coils and in the rotor; the evaluation of AC losses in the stator coils; the shape of the high-temperature superconductor tape stacks used in the rotor instead of permanent magnets, and the issue of the demagnetization of those stacks; the cryogenic topology and the conceptual study on future integration of cryogenic supply in airborne applications; the power electronics. At the time of writing (December 2019), the ASuMED motor is being assembled and will be tested in the first months of 2020. Reports on the test results will be communicated

through future publications and on the project's website [24].

Acknowledgments
This work was funded by the European Commission Grant No 723119 (ASuMED). The authors acknowledge K&S GmbH Projektmanagement for the excellent coordination of the project. SuperOx acknowledges the support from Ministry of Science and Higher Education of Russia, Grant 075-11-2018-176 (unique identification number RFMEFI58818X0009).

References

[1] 2011 Flightpath 2050 Europe's Vision for Aviation Tech. rep. EUROPEAN COMMISSION Directorate-General for Research and Innovation, Directorate General for Mobility and Transport URL https://doi.org/10.2777/50266
[2] Luongo C A, Masson P J, Nam T, Mavris D, Kim H D, Brown G V, Waters M and Hall D 2009 *IEEE Transactions on Applied Superconductivity* **19** 1055–1068
[3] Lee S, Petrykin V, Molodyk A, Samoilenkov S, Kaul A, Vavilov A, Vysotsky V and Fetisov S 2014 *Superconductor Science and Technology* **27** 044022
[4] Chepikov V, Mineev N, Degtyarenko P, Lee S, Petrykin V, Ovcharov A, Vasiliev A, Kaul A, Amelichev V, Kamenev A, Molodyk A and Samoilenkov S 2017 *Superconductor Science and Technology* **30** 124001
[5] Lao M, Hänisch J, Kauffmann-Weiss S, Gehring R, Fillinger H, Drechsler A and Holzapfel B 2019 *Review of Scientific Instruments* **90** 015106
[6] Lao M, Willa R, Meledin A, Rijckaert H, Chepikov V, Lee S, Petrykin V, Driessche I V, Molodyk A, Holzapfel B and Hänisch J 2019 *Superconductor Science and Technology* **32** 094003
[7] Ovcharov A V, Degtyarenko P N, Chepikov V N, Vasiliev A L, Gavrilkin S Y, Karateev I A, Tsvetkov A Y and Kaul A R 2019 *Scientific Reports* **9** 15235
[8] Pardo E, Šouc J and Frolek L 2015 *Superconductor Science and Technology* **28** 044003
[9] Pardo E, Grilli F, Liu Y, Wolftaedler S and Reis T 2019 *IEEE Transactions on Applied Superconductivity* **29**
[10] Nishioka T, Amemiya N, Enomoto N, Jiang Z, Yamada Y, Izumi T, Shiohara Y, Saitoh T, Iijima Y and Kakimoto K 2005 *IEEE Transactions on Applied Superconductivity* **15** 2843–2846
[11] Tsukamoto O 2005 *Superconductor Science and Technology* **18** 596–605
[12] Grilli F, Brambilla R and Martini L 2007 *IEEE Transactions on Applied Superconductivity* **17** 3155–3158
[13] Solovyov M, Pardo E, Souc J, Gömöry F, Skarba M, Konopka P, Pekarčíková M and Janovec J 2013 *Superconductor Science and Technology* **26** 115013
[14] Perez A, van der Woude R R and Dekker R 2019 *IOP Conference Series: Materials Science and Engineering* **502** 012139
[15] Kapolka M, Pardo E, Grilli F, Baskys A, Climente-Alarcon V and Glowacki B A 2019 *Superconductor Science and Technology* (in press, doi: 10.1088/1361-6668/ab5aca)
[16] Climente-Alarcon V, Smara A, Patel A, Glowacki B A, Baskys A and Reis T 2019 *Proceedings of the AIAA Propulsion and Energy Forum, 19–22 August 2019, Indianapolis, Indiana, USA*
[17] Dadhich A, Kapolka M, Pardo E, Climente-Alarcon V, Smara A, Mineev N, Tomkow L, Glowacki B A and Grilli F 2019 *Proceedings of the 14^{th} European Conference on Applied Superconductivity* (doi:10.5281/zenodo.3557354)
[18] Smara A, Mineev N, Climente-Alarcon V, Patel A, Baskys A, Glowacki B A and Reis T 2019 *Superconductor Science and Technology* **32** 085009
[19] Kowalski T 2019 *Mess- und Betriebsverfahren von stromrichtergespeisten Drehfeldmaschinen mit supraleitender Statorwicklung* Ph.D. thesis Technische Hochschule Aschaffenburg
[20] Mõlder H, Vinnal T and Beldjajev V 2010 *Proceedings of the 2010 Electric Power Quality and Supply Reliability Conference* 143–150 URL https://doi.org/10.1109/PQ.2010.5550006
[21] Shamsi-Nejad M, Nahid-Mobarakeh B, Pierfederici S and Meibody-Tabar F 2010 *Proceedings of the 2010 IEEE Vehicle Power and Propulsion Conference* 1–6 URL https://doi.org/10.1109/VPPC.2010.5729031
[22] Büdel J, Teizelkötter J and Stock A 2019 *Proceedings of the 21^{th} European Conference on Power Electronics and Applications (EPE '19 ECCE Europe)* 1–10 URL https://doi.org/10.23919/EPE.2019.8915524
[23] Stock A, Teizelkötter J, Büdel J and Staudt S 2018 *Proceedings of the 20^{th} European Conference on Power Electronics and Applications (EPE '18 ECCE Europe)* 1–9 URL https://ieeexplore.ieee.org/document/8515600
[24] ASuMED – Advanced Superconducting Motor Experimental Demonstrator. http://asumed.oswald.de/